

Formation of metastable atomic hydrogen in the $2s$ state from symmetry-resolved doubly excited states of molecular hydrogen

Takeshi Odagiri,^{1,*} Yoshiaki Kumagai,¹ Motoyoshi Nakano,¹ Takehiko Tanabe,¹ Isao H. Suzuki,^{2,3} Masashi Kitajima,¹ and Noriyuki Kouchi¹

¹*Department of Chemistry, Tokyo Institute of Technology, Tokyo 152-8551, Japan*

²*National Institute of Advanced Industrial Science and Technology (AIST), Tsukuba 305-8568, Japan*

³*Photon Factory, Institute of Materials Structure Science, KEK, Tsukuba 305-0801, Japan*

(Received 16 June 2011; published 2 November 2011)

The cross sections for the formation of the metastable atomic hydrogen in the $2s$ state in photoexcitation of H_2 and D_2 were measured as a function of the incident photon energy in the range of the doubly excited states with their symmetries of the electronic states, $^1\Sigma_u^+$ or $^1\Pi_u$, being resolved. It has turned out from the comparison with the cross-section curves for other dissociation processes and the theoretical calculation [J. D. Bozek *et al.*, *J. Phys. B* **39**, 4871 (2006)] that the $Q_2^1\Pi_u(1)$ doubly excited state of H_2 dissociates into both $H(2s) + H(2p)$ and $H(2p) + H(2p)$. The dissociation dynamics of this state has been discussed in terms of the nonadiabatic transition during neutral dissociations.

DOI: 10.1103/PhysRevA.84.053401

PACS number(s): 33.80.Gj

I. INTRODUCTION

Doubly excited states of molecules are short-lived resonance states which decay through autoionizations and neutral dissociations. Since the wave function of such molecular resonance states cannot simply be described by the Born-Oppenheimer products due to mixing between discrete and continuum configurations [1,2], the dynamics of the formation and decay of them has attracted many theoretical and experimental investigations, especially for molecular hydrogen as summarized in review papers [3,4]. Figure 1 shows the theoretical potential energy curves of the doubly excited states of H_2 [5,6]. The dynamics, however, has not been fully understood even in this simple molecule. For example, a peak due to an optically forbidden doubly excited state of H_2 and D_2 in the electron energy loss spectra tagged with the $H(2p)$ or $D(2p)$ fragment formation measured by our group has not yet been explained theoretically and the origin of the peak remains an open question [8–11]. There also exists a disagreement in the discussion on the dynamics of the neutral dissociation of the lowest and second-lowest $^1\Pi_u$ states in the Q_2 series, i.e., the $Q_2^1\Pi_u(1)$ and $Q_2^1\Pi_u(2)$ states of H_2 , which we concern with in the present study. In the following, the previous investigations on the dissociation dynamics of the $Q_2^1\Pi_u(1, 2)$ states are summarized.

The $Q_2^1\Pi_u(1)$ and $Q_2^1\Pi_u(2)$ states, of which the main configurations near the equilibrium internuclear distance in the ground electronic state are $(2p\pi_u, 2s\sigma_g)$ and $(2p\pi_u, 3d\sigma_g)$, respectively [6], are known to dissociate into $H(2s) + H(2p)$ and $H(2p) + H(2p)$, respectively [4,12]. Misakian and Zorn [13] measured the excitation function for the production of fast $H(2s)$ fragments (kinetic energy > 2 eV) in electron- H_2 collisions and observed a threshold for the production of the fast $H(2s)$ fragments at the electron impact energy of approximately 29 eV. From the energy conservation and the measured angular distribution of the fast $H(2s)$ fragments at 41.5-eV incident electron energy, they concluded that the

formation of the fast $H(2s)$ atoms proceed via a $^1\Pi_u$ state in the Q_2 series of the doubly excited states of H_2 [13]. The theoretical calculations on the velocity distribution of $H(2s)$ fragments due to the $Q_2^1\Pi_u(1)$ state of H_2 [14] and on the potential energy of the $Q_2^1\Pi_u(1)$ state at the internuclear distance of 1.8 a.u. [15] were reasonably consistent with the experimental results by Misakian and Zorn [13]. Thus, a consensus that the precursor state of the fast $H(2s)$ fragment is the $Q_2^1\Pi_u(1)$ state has been developed. Because the state was also known as the main contributor to the cross section for the $H(2p)$ atom formation [16–19], the $Q_2^1\Pi_u(1)$ state has been considered to dissociate into $H(2s) + H(2p)$. However, this conclusion needs to be re-examined since (i) the theoretical potential energies and resonance widths of the doubly excited states of H_2 by the recent calculation with large configuration bases [6] differ from those by the former calculation [15] and (ii) the velocity distributions of $H(2s)$ fragments depend on the electron impact energy [20], showing a possibility of contributions from the neutral and ionic molecular states other than the $Q_2^1\Pi_u(1)$ state in the electron collision experiment by Misakian and Zorn. In the recent measurement of the cross sections for the $H(2s)$ atom formation in photoexcitation of H_2 it was concluded that the contribution of the $Q_2^1\Pi_u(1)$ state of H_2 was not so large [4,21] (see Fig. 3).

On the other hand, the $Q_2^1\Pi_u(2)$ state was concluded to dissociate into $H(2p) + H(2p)$ because the excitation spectrum of the simultaneous emission of two Lyman- α photons in photoexcitation of H_2 [22] were well reproduced by the calculated photoabsorption or photodissociation profiles due to the $Q_2^1\Pi_u(2)$ state [4,19]. However, the excitation spectrum of Ref. [22] does not agree with the recent one by Odagiri *et al.* [23], the latter of which is more reliable [23]. Odagiri *et al.* [23] found that the precursor doubly excited state for the formation of two $H(2p)$ atoms is the $Q_2^1\Pi_u(1)$ state, which disagrees with the argument above.

To investigate the precursor doubly excited states resulting in the formation of $H(2s)$ fragments it is necessary to measure the cross sections of the process as a function of excitation energy rather than the electron impact energy as was previously

*odagiri.t.aa@m.titech.ac.jp

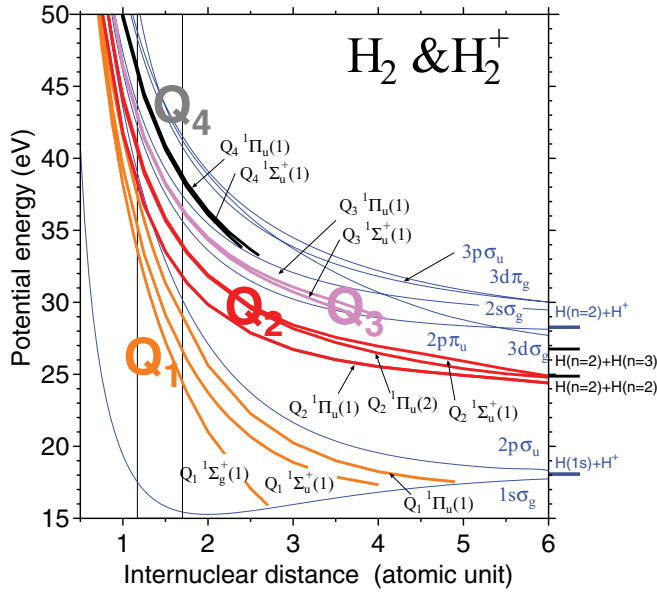


FIG. 1. (Color online) The potential energy curves of the doubly excited states of H_2 (Refs. [5,6], thick solid curves) and H_2^+ (Ref. [7], thin solid curves). The Franck-Condon region of H_2 is indicated by the vertical lines. The origin of the potential energy is taken at the lowest vibrational-rotational level in the ground electronic state of H_2 .

done [13,20]. As mentioned above, Glass-Maujean *et al.* [21] measured cross sections for $H(2s)$ formation in photoexcitation, σ_{2s} , of H_2 by using the detection technique based on the collision-induced emission of the Lyman- α photons [$H(2s) + H_2 \rightarrow H(1s) + H_2 + \text{Lyman-}\alpha \text{ photon}$] in a gas cell filled with relatively high pressure. However, it required fitting procedures to the experimental time-dependent Lyman- α intensity curves for obtaining the cross sections [21], and, thus, the number of measured points was small and the error bars were relatively large. Recently, we have developed a method to measure the cross sections for the $H(2s)$ formation from symmetry-resolved excited states formed in photoexcitation of linear molecules [24]. The principle of measuring the symmetry-resolved cross-section curves is as follows. Within the dipole approximation, the angle differential cross section for $H(2s)$ formation is given by

$$d\sigma_{2s}/d\Omega = (\sigma_{2s}/4\pi)[1 + \beta(3\cos^2\theta - 1)/2], \quad (1)$$

where θ is the angle of the fragment ejection with respect to the electric field vector of the incident light and β is the asymmetry parameter when the dissociations occur rapidly as compared with the time scale of the molecular rotation (the axial recoil approximation) [25]. For the $\Sigma \rightarrow \Sigma$ transitions $\beta = 2$ and for the $\Sigma \rightarrow \Pi$ transitions $\beta = -1$. Hence, the integral cross sections due to $\Sigma \rightarrow \Sigma$ and $\Sigma \rightarrow \Pi$ transitions, σ_{2s}^{Σ} and σ_{2s}^{Π} , are obtained separately if the measurements are done for the case of fragment ejection in parallel to the electric field vector of the incident light ($\theta = 0^\circ$) and perpendicular to it ($\theta = 90^\circ$), respectively. In the present study this method is applied to H_2 and D_2 . The formation and decay dynamics of the doubly excited states of molecular hydrogen leading to the formation of the metastable atomic hydrogen in the $2s$

state are investigated with their symmetries being resolved. A discussion on the dynamics of neutral dissociations of the doubly excited states of H_2 and D_2 is given with special attention to those of the $Q_2^1\Pi_u$ states.

II. EXPERIMENTAL

The experiments were carried out at the undulator beam line 28B of the photon factory, KEK. A linearly polarized photon beam from the variable-included-angle Monk-Gillieson monochromator [26] was introduced into the gas cell filled with molecular hydrogen. The metastable hydrogen atom in the $2s$ state produced through photoexcitation of molecular hydrogen was detected by the combination of a localized electric field created by a stack of parallel plate electrodes and a detector of photons that is composed of a microchannel plate (MCP) coated with CsI and an MgF_2 window in front of it. The $2s$ state of atomic hydrogen mixes with the $2p$ state by the Stark effect due to the electric field and the atom decays to the ground state by emitting a Lyman- α photon, which was detected by the photon detector. An angle-resolved detection of the metastable hydrogen atoms was achieved by putting the stack of parallel plate electrodes 100 mm away from the center of the gas cell, as shown in Fig. 2. With the optimized strength of the electric field (42 V cm^{-1}) the metastable hydrogen atoms having a kinetic energy of 0.01–10 eV decay within approximately 2 mm of the leading edge of the plates. The gas cell and the detector system were rotated around the beam axis (X axis in Fig. 2) to change the angle of detection, θ_d , as shown in Figs. 2(a) and 2(b), where the detection system is placed in parallel [$\theta_d = 0^\circ$; Fig. 2(a)] with the electric field vector of the incident light (Z axis in Fig. 2) and perpendicular to it [$\theta_d = 90^\circ$; Fig. 2(b)]. In principle, integral cross sections for the formation of the metastable atomic hydrogen due to the $\Sigma \rightarrow \Sigma$ and $\Sigma \rightarrow \Pi$ transitions, σ_{2s}^{Σ} and σ_{2s}^{Π} , can be obtained from the counting rates of the metastable hydrogen atoms measured at the parallel and perpendicular detector orientation, $N_{2s}(\theta_d = 0^\circ)$ and $N_{2s}(\theta_d = 90^\circ)$, respectively, by normalizing them for the number density of the target molecule and flux of the incident photon as described by Eq. (6) of our previous paper [24]. However, a correction was necessary to eliminate the small contamination from the other symmetry originating

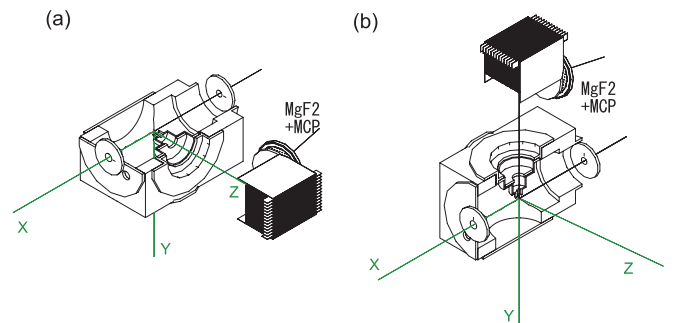


FIG. 2. (Color online) The gas cell and the detector for the metastable hydrogen atoms in the $2s$ state; (a) “parallel” orientation ($\theta_d = 0^\circ$) and (b) “perpendicular” orientation ($\theta_d = 90^\circ$). The space-fixed X and Z axes are parallel to the propagation direction and the electric field vector of the linearly polarized incident light, respectively.

from the geometry of the detector, finite angular resolution, and finite collision volume. These effects were evaluated by a numerical simulation and the following relations were obtained: $\dot{N}_{2s}(\theta_d = 0^\circ) \propto 8.71 \times \sigma_{2s}^\Sigma + 9.08 \times 10^{-2} \times \sigma_{2s}^\Pi$ and $\dot{N}_{2s}(\theta_d = 90^\circ) \propto 6.25 \times 10^{-2} \times \sigma_{2s}^\Sigma + 4.70 \times \sigma_{2s}^\Pi$. The contaminations are generally small but in $\dot{N}_{2s}(\theta_d = 0^\circ)$ it was not negligible, because the relation $\sigma_{2s}^\Sigma(E) \ll \sigma_{2s}^\Pi(E)$ was obtained for the present incident photon energy E , as is shown in the next section. The cross sections were put on the absolute scale by normalizing the sum of the $\sigma_{2s}^\Sigma(E)$ and $\sigma_{2s}^\Pi(E)$ cross sections for H_2 to those obtained by Glass-Maujean *et al.* [21] (see the next section). The flux of the incident photons was monitored at the exit of the gas cell by using an Au plate of which sensitivity was measured, prior to the experiments, by using an NIST-calibrated silicon photodiode (model AXUV-100G, IRD Inc., Saskatoon, Canada).

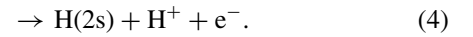
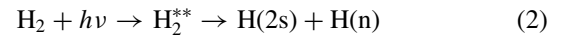
On the gas cell another photon detector that is composed of an MgF_2 window and an MCP (not shown in Fig. 2) was mounted for detection of Lyman- α photons produced near the collision region, i.e., the Lyman- α photons from short-lived $H(2p)$ or $D(2p)$ atoms produced in photoexcitation. Cross sections for the $H(2p)/D(2p)$ formation differential with respect to the solid angle of the emitted photons, $d\sigma_{2p}/d\Omega$, were obtained as a function of E from counting rates of the photon detector normalized for the number density of the target molecule and flux of the incident photon. Anisotropy of the photon emission was found to be low and thus the $d\sigma_{2p}/d\Omega$ differential cross sections as a function of E give the integral cross sections $\sigma_{2p}(E)$ in a relative scale. The $\sigma_{2p}(E)$ cross sections were put on the absolute scale by normalizing them to the theoretical cross sections [12,27] (see the next section). The measurements of the $\sigma_{2p}(E)$ and one of the σ_{2s}^Σ and σ_{2s}^Π cross sections were done simultaneously. There is also a retarding type electron energy-analyzer on the other side of the gas cell (also not shown in Fig. 2). Using this electron detector, we measured the photoelectron angular distribution (PAD) for obtaining the Stokes parameter \bar{S}_1 of the linear polarization and the tilt angle λ of the polarization ellipse [28] of the incident light. Through the measurement of the PAD we checked the alignment of the apparatus against the incident light beam. The polarization degree of the incident light was approximately 0.94 by measuring the PAD from He at the 50-eV incident photon energy. The electron detector was also operated as a detector for ions with thermal energy by changing voltages applied to electrodes inside. The photoion yield from He and Ne were measured as a function of the wavelength of incident light by using this ion detector, and these yield curves were utilized for the wavelength calibration of the incident light. The bandpass of the incident light was approximately 1.5×10^{-2} nm at 27.2 nm (energy width of approximately 25 meV at a 45.6-eV incident photon energy). Measurements were done at the pressure of the gas cell below 0.12 Pa where the counting rates of the metastable hydrogen atoms and the Lyman- α photons were proportional to the pressure. Further details of the experiments were described previously [24].

It is important to discuss a contribution from the reaction of $H(3p) \rightarrow H(2s) + \text{Balmer-}\alpha$ photon in the $H(2s)$ atom signals. The cross sections for the emission of Balmer- α fluorescence [$H(3s,3p,3d) \rightarrow H(n=2) + \text{Balmer-}\alpha$ photon] in photoexcitation of H_2 , $\sigma_{\text{Bal}\alpha}$, were measured previously

and they reached a maximum value of approximately 5.5×10^{-3} Mb around the incident photon energy of 36–38 eV [29] (1 Mb = 1×10^{-18} cm²). As is shown below, the σ_{2s}^Σ and σ_{2s}^Π cross sections for H_2 at this energy range were approximately 7×10^{-3} and $6\text{--}8 \times 10^{-2}$ Mb, respectively, the former of which is comparable to the maximum of the $\sigma_{\text{Bal}\alpha}$ cross sections. However, evidence of $H(3p) \rightarrow H(2s)$ fluorescence was hardly found in the decay curve analysis for the time-resolved detections of the Balmer- α fluorescence in the range of the doubly excited states [30], and, thus, the contribution of the above transition would be small even in the σ_{2s}^Σ cross sections.

III. RESULTS AND DISCUSSION

The metastable $H(2s)$ atoms are formed in the photoexcitation of H_2 through the following processes:



They are neutral dissociations [process (2)] and autoionizations [process (3)] of the doubly excited states of H_2 (H_2^{**}) and direct-dissociative photoionizations [process (4)]. Because the final state of processes (3) and (4) are the same, the cross sections due to these processes must be added coherently. As mentioned below, the ionic states contributing to processes (3) and (4) are the $H_2^+(2s\sigma_g)$ and $H_2^+(3p\sigma_u)$ states [12]. From the potential energy curves in Fig. 1, the doubly excited states involved in process (3) can probably be the Q_4 states or higher states since they must have higher energy than the final ionic states. Thus, the contribution from process (3) in $2s$ -atom formation is expected to be smaller than those from processes (2) and (4) since photoexcitation to such high energy states would be less probable.

Sum of the symmetry-resolved cross sections, $\sigma_{2s}^\Sigma(E) + \sigma_{2s}^\Pi(E)$, gives symmetry-unresolved cross sections, $\sigma_{2s}(E)$, since the dipole selection rule allows only $^1\Sigma_u^+$ and $^1\Pi_u$ as the excited state symmetries in the photoexcitation of molecular hydrogen from its ground electronic state ($^1\Sigma_g^+$). In Fig. 3, the present $\sigma_{2s}(E)$ curve of H_2 are shown together with that obtained by Glass-Maujean *et al.* [21]. The present data are normalized to the previous one [21] so the sum of the squared residuals between the two data sets in the range 36–38 eV is a minimum. Gross features of the two cross-section curves are similar but the peak lies around 35.6 eV in the present cross sections while it lies around 37 eV in the previous ones [21]. It is noted that the present measurements contain no fitting procedure that is involved in the previous study to obtain each data point in Fig. 3 [21] (see Sec. I) and, thus, the shape of the present cross-section curve seems to be more reliable. The structure of the previous cross-section curve [21] was attributed to neutral dissociation of the Q_1 $^1\Sigma_u^+(2)$, Q_2 $^1\Pi_u(1, 4, \text{ and } 5)$, and Q_3 $^1\Pi_u(1)$ doubly excited states of H_2 and the dissociative photoionization to $H_2^+(2s\sigma_g) + e^-$ based on the semiclassical calculation [4] as shown in Fig. 3. The semiclassical cross sections due to the neutral dissociations in Fig. 3 were obtained from the Franck-Condon (FC) factors between the ground electronic

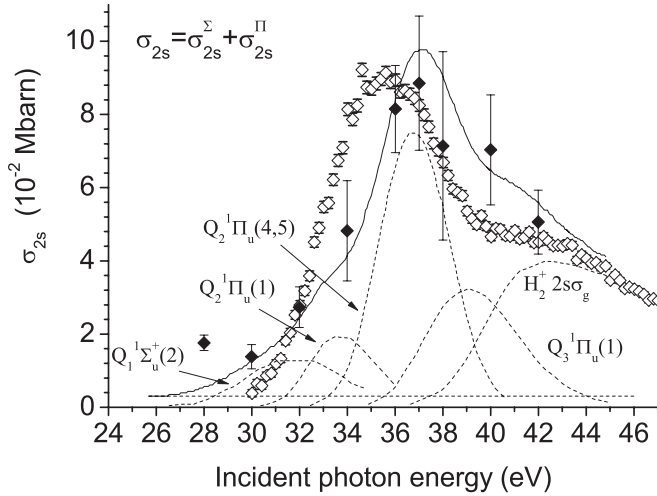


FIG. 3. The symmetry-unresolved cross sections for the $2s$ -atom formation of H_2 ; (open diamonds) present data; (solid diamonds) data of Ref. [21]. The present data were normalized to the data of Ref. [21] in the range 36–38 eV (see text). Solid curve represents the theoretical fit [4] to the experimental data of Ref. [21] and dashed curves represent the various contributions to the solid curve.

state and the doubly excited states of H_2 multiplied by constant factors while the semiclassical cross sections due to the dissociative photoionization in Fig. 3 was obtained from the FC factors between the ground state of H_2 and the $(2s\sigma_g)$ state of H_2^+ combined with the Born approximation for the ionization multiplied by a constant factor [4]. The physical meanings of the constant factors, which were practically used as fitting parameters, are the electric dipole moment squared and branching ratio of the $2s$ -atom formation. Thus, they were approximated as energy independent in the semiclassical model [4]. Although the semiclassical cross section does not fit the present data, a better fit could be obtained if a suitable parameter set is used. For a more detailed discussion, however, we compared our symmetry-resolved cross-section curves with a full quantum-mechanical calculation as follows.

Figure 4 shows the symmetry-resolved cross sections for the formation of the metastable atomic hydrogen in the $2s$ state, $\sigma_{2s}^\Sigma(E)$ and $\sigma_{2s}^\Pi(E)$, in photoexcitation of H_2 and D_2 . The vertical scales were put on the absolute scale through the normalization in Fig. 3. It has turned out that for both H_2 and D_2 $\sigma_{2s}^\Sigma(E)$ are much smaller than $\sigma_{2s}^\Pi(E)$, revealing dominant contributions of the $^1\Sigma_g^+ \rightarrow ^1\Pi_u$ transitions in the metastable $2s$ -atom formation. A large isotope effect is seen in the $\sigma_{2s}^\Pi(E)$ curve below 46 eV [see Fig. 4(b)], while a relatively small difference is seen between the $\sigma_{2s}^\Sigma(E)$ curves of the two isotopes [see Fig. 4(a)]. The tendency of the smaller cross sections for D_2 than those for H_2 is understandable by taking into account that a longer time period is needed for molecular dissociations in D_2 and, thus, fewer molecules in doubly excited states of D_2 decay through neutral dissociation escaping from autoionizations than in H_2 . Therefore, the isotope effect in the σ_{2s}^Π cross sections show the contributions from neutral dissociations [process (2)] of the $^1\Pi_u$ doubly excited states up to 46 eV. From the theoretical potential energy curves of Fig. 1 neutral dissociations above approximately

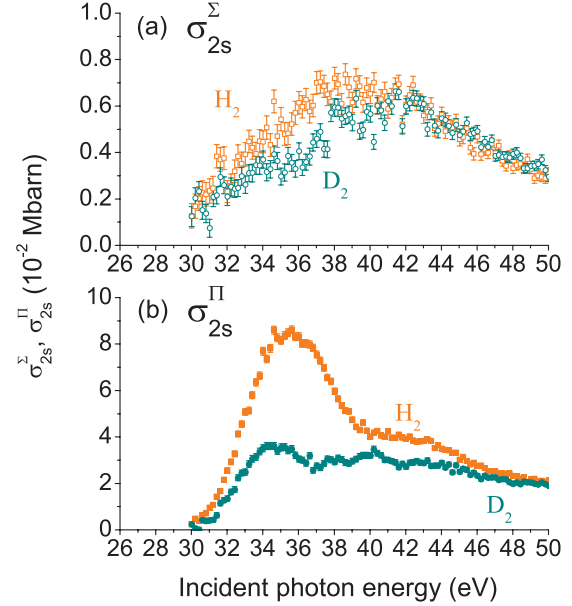


FIG. 4. (Color online) The symmetry-resolved cross sections for the $2s$ -atom formation in photoexcitation of H_2 and D_2 ; (a) the cross sections for the $^1\Sigma_u^+$ symmetry and (b) the cross sections for the $^1\Pi_u$ symmetry [(open and solid squares) H_2 ; (open and solid circles) D_2].

40 eV are likely to proceed via the Q_3 and Q_4 doubly excited states.

On the other hand, almost no isotope effect appears in the range above 46 eV for both $\sigma_{2s}^\Sigma(E)$ and $\sigma_{2s}^\Pi(E)$. Around this energy the direct-dissociative photoionizations (DPI) leading to the metastable $2s$ -atom formation, whose thresholds are above 38 eV [12,27], dominate the cross sections since photoexcitation to doubly excited states lying in such a high energy range would be less probable (see Fig. 1). Two ionic states correlating to the dissociation limit of $H(2s) + H^+$ are known: the $H_2^+(2s\sigma_g)$ and $H_2^+(3p\sigma_u)$ states [12]. Thus, the DPI included in the $\sigma_{2s}^\Sigma(E)$ curve are the $(2s\sigma_g)(\varepsilon\sigma_u)$ and $(3p\sigma_u)(\varepsilon\sigma_g)$ channels while those included in the $\sigma_{2s}^\Pi(E)$ curve are the $(2s\sigma_g)(\varepsilon\pi_u)$ and $(3p\sigma_u)(\varepsilon\pi_g)$ channels, where $(\varepsilon\sigma_{g,u})$ and $(\varepsilon\pi_{g,u})$ indicate the ionized electrons. The $\Sigma:\Pi$ ratios at 50 eV were obtained to be 0.14 for H_2 and 0.17 for D_2 .

The cross sections in the energy range below 46 eV are dominated by the neutral dissociation of the $^1\Sigma_u^+$ and $^1\Pi_u$ doubly excited states of H_2 and D_2 (see comparisons between the experimental and theoretical cross sections in Fig. 5). Referring to the Barat-Lichten (BL) rule to correlate diabatically between the molecular states and separated atoms limits, only the $Q_1^1\Sigma_u^+(1)$ and $Q_2^1\Pi_u(1)$ doubly excited states are responsible for the $2s$ -atom formation [12]. In Fig. 5, we compared the present experimental data with the theoretical photodissociation cross sections for the $2s$ -atom formation obtained by solving the time-dependent Schrödinger equation [12,27]. It is noted that the theory calculated the populations that remained in the doubly excited states without being autoionized for the photodissociation cross sections and the dissociation products were determined following to the BL correlation rule [12,19]. Thus, they took account of the neutral dissociation of the $Q_1^1\Sigma_u^+(1)$ and $Q_2^1\Pi_u(1)$ doubly excited states [process (2)] and the DPI to the $2s\sigma_g$ and $3p\sigma_u$ states

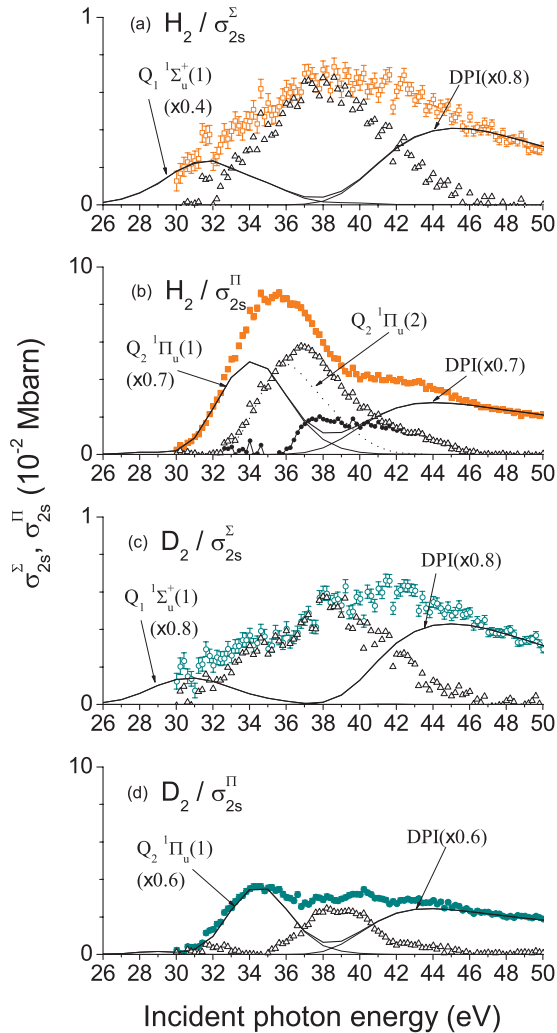


FIG. 5. (Color online) The symmetry-resolved cross sections for the formation of metastable atomic hydrogen in the $2s$ state; (a) σ_{2s}^{Σ} for H_2 , (b) σ_{2s}^{Π} for H_2 , (c) σ_{2s}^{Σ} for D_2 , and (d) σ_{2s}^{Π} for D_2 (the present data are the same as those in Fig. 4). The theoretical cross sections for the $2s$ -atom formation due to the $Q_1 \ ^1\Sigma_u^+(1)$, $Q_2 \ ^1\Pi_u(1)$, and DPI [12,27] multiplied by the factors indicated are shown by thin solid curves and sum of them are shown by thick solid curves (see text). The differences between the experimental and normalized theoretical cross sections are shown by open triangles. The theoretical photodissociation cross sections due to the $Q_2 \ ^1\Pi_u(2)$ state normalized to the open triangles are shown by the dotted curve in (b). The differences between the open triangles and the dotted curve are represented by the solid curve with dots in (b).

of the hydrogen molecular ion [process (4)] in the theoretical calculation for the $2s$ -atom formation [12,19,27]: the lower energy humps of the theoretical curves in Figs. 5(a)–5(d) originate from the neutral dissociations of the doubly excited states and the higher ones are due to the DPI. Individual components of the theoretical cross sections were multiplied by the factors indicated in Fig. 5 and summed so they (thick solid curves in Fig. 5) agree well with the present experimental ones in the range 30–32 eV and 46–50 eV. Despite the normalization, the relation $\sigma_{2s}^{\Pi}(E) \gg \sigma_{2s}^{\Sigma}(E)$ is reproduced in the theoretical results for both H_2 and D_2 . The onset around

30 eV in the experimental Π cross sections in Figs. 5(b) and 5(d) are also reproduced well in the theoretical cross-section curves leading to the conclusion that the $Q_2 \ ^1\Pi_u(1)$ doubly excited state contributes largely in the $2s$ -atom formation for both H_2 and D_2 . Note that the photodissociation cross sections due to the second lowest $^1\Pi_u$ state in the Q_2 series, the $Q_2 \ ^1\Pi_u(2)$ state, are expected to rise above 32 eV [12,27] (see also the absorption profile shown in Fig. 2(b) of Ref. [4]), and, thus, the onset around 30 eV cannot be attributed to the $Q_2 \ ^1\Pi_u(2)$ state. As seen in Fig. 5 the theoretical cross sections do not reproduce the experimental ones in the range 32–46 eV. Differences between them are attributed to contributions from the higher doubly excited states and are indicated by open triangles in Fig. 5. It is clear that the doubly excited states other than those connected to the dissociation limit of $H(2s) + H(nl)$ by the BL correlation rule also contribute largely to the experimental cross sections.

Figures 6(b) and 6(c) show the photodissociation cross sections for the $2p$ -atom formation, σ_{2p} , measured in the present study. The present $\sigma_{2p}(E)$ curves of H_2 and D_2 were normalized to the theoretical ones [12,27] in the range of the DPI (48–50 eV). Note that the experimental cross-section ratio between H_2 and D_2 is maintained in the normalization. The solid circles in the figures are the $\sigma_{2p}(E)$ curves of H_2 and D_2 which were measured and then normalized to the theoretical

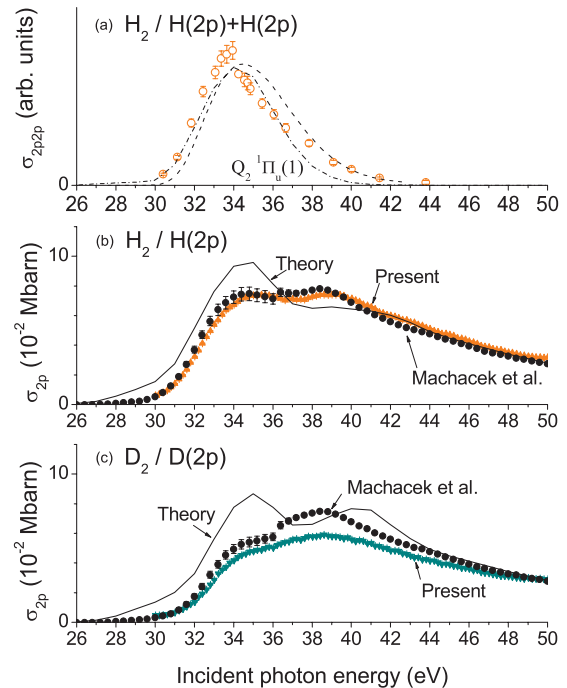


FIG. 6. (Color online) (a) The cross sections for the formation of two $H(2p)$ atoms [23] (see text). [(b) and (c)] The cross sections for the $H(2p)/D(2p)$ atom formation in photoexcitation of H_2 (b) and D_2 (c); (solid triangles) present results; (solid circles) the previous experimental results [31]; (solid curves) the theoretical results [12,27]. The photodissociation cross sections due to the $Q_2 \ ^1\Pi_u(1)$ doubly excited state of H_2 calculated through solving the time-dependent Schrödinger equation (Refs. [12,27], dot-dashed curve) and with the semiclassical approximation (Ref. [23], dashed curve) are also shown in (a).

cross sections by Machacek *et al.* [31]. The two experimental data agreed well with each other and also agree fairly well with the theoretical curves. The theory includes contributions from the $Q_1^1 \Sigma_u^+(2)$, $Q_1^1 \Pi_u(1)$, $Q_2^1 \Sigma_u^+(1-6)$, and $Q_2^1 \Pi_u(1-7)$ doubly excited states and the $2p\pi_u$, $3d\sigma_g$, and $3d\pi_g$ ionic channels [12], all of which correlate to the states including the $2p$ -atom at the separated atoms limits by the BL rule [12,27]. Among them, the $Q_2^1 \Pi_u(1)$ state is the main contributor to the $\sigma_{2p}(E)$ [19,27].

In Fig. 6(a) we show our previous experimental results of the coincidence detection of two Lyman- α photons in photoexcitation of H₂ [23]. It is the cross section for the formation of two H($2p$) atoms differential with respect to each solid angle for the two Lyman- α photons from them as a function of E . Although the recent investigations revealed the remarkable angular correlation of the two Lyman- α photons [32–35], the angular correlation pattern does not seem to change quite so much with the incident photon energy since one $^1\Pi_u$ state dominantly contributes to the formation of two H($2p$) atoms, as mentioned below. Thus, Fig. 6(a) shows the integral cross sections for the formation of two H($2p$) atoms against E , $\sigma_{2p2p}(E)$, in a relative scale. Odagiri *et al.* [23] attributed the main peak in Fig. 6(a) to the neutral dissociation of the $Q_2^1 \Pi_u(1)$ state of H₂ based on the semiclassical calculation of $\sigma_{2p2p}(E)$, of which the result is shown in Fig. 6(a) by the dashed curve. The photodissociation cross section due to the $Q_2^1 \Pi_u(1)$ state was calculated in a more sophisticated way [12,27] and the result is shown by the dot-dashed curve in Fig. 6(a), which supports the conclusion by Odagiri *et al.* [23]. Hence, it is concluded that the precursor doubly excited states for the photodissociation into H($2p$) + H($2p$) is the $Q_2^1 \Pi_u(1)$ doubly excited state of H₂.

In summary, in the three cross sections above, i.e., the $\sigma_{2s}^\Pi(E)$, $\sigma_{2p}(E)$, and $\sigma_{2p2p}(E)$ cross sections, we found a large contributions of the $Q_2^1 \Pi_u(1)$ doubly excited state which is the lowest $^1\Pi_u$ state in the Q_2 series. Thus, it has turned out that the $Q_2^1 \Pi_u(1)$ doubly excited state of H₂ dissociates into both of H($2p$) + H($2p$) and H($2s$) + H($n = 2$), which is clear evidence of the coupling between the dissociation channels. Such coupling was not taken into account in the theory [12,27].

Many avoided crossings have been found between the potential energy curves of the doubly excited states [6,36], where nonadiabatic transitions between states can occur depending on the coupling strength and velocity of the relative motion of two nuclei at the avoided crossing [37]. It is, thus, possible that the doubly excited states which are not connected to the H($2s$) + H($n\ell$) dissociation limit by the BL correlation rule also contribute to the $2s$ -atom formation. One such doubly excited state would be the $Q_2^1 \Pi_u(2)$ state that correlates to H($2p$) + H($2p$) following the BL correlation rule. Sanchez and Martin [6] reported an avoided crossing between the potential energy curves of the $Q_2^1 \Pi_u(1)$ and $Q_2^1 \Pi_u(2)$ states at the internuclear separation of approximately 5 a.u. In Fig. 5(b) the dotted curve shows the theoretical photodissociation cross section via the $Q_2^1 \Pi_u(2)$ state [12,27] with its absolute value being normalized to the difference curve represented by the open triangles. The onset around 32 eV in the difference curve in Fig. 5(b) agrees well with the theoretical photodissociation curve due to the $Q_2^1 \Pi_u(2)$ state. Thus, the $Q_2^1 \Pi_u(2)$ state

TABLE I. Oscillator strengths ($\times 10^{-4}$) in the range 30–50 eV for the formation of the metastable atomic hydrogen in the $2s$ state in photoexcitation of H₂ and D₂.

	H ₂	D ₂		
Σ	$Q_1^1 \Sigma_u^+(1)$	1.1	0.5	
	Difference (Δ)	4.6	3.9	
	DPI	3.2	3.4	
	Sum	8.9	7.7	
Π	$Q_2^1 \Pi_u(1)$	21	14	
	Difference (Δ)	$Q_2^1 \Pi_u(2)$	20	—
		Others	12	12
	DPI	24	21	
	Sum	77	47	

seems to contribute largely to the σ_{2s}^Π cross sections of H₂. It is remarkable that the $Q_2^1 \Pi_u(2)$ state gives a contribution comparable with the $Q_2^1 \Pi_u(1)$ state in the σ_{2s}^Π cross sections of H₂. The difference between the open triangles and the dotted curve in Fig. 5(b) is shown by the solid curve with dots. On the other hand, the difference curve of D₂ in Fig. 5(d) rises around 35 eV, indicating the contribution due to the $Q_2^1 \Pi_u(2)$ state is not so large in the σ_{2s}^Π cross sections of D₂. Origins of the rests of the cross sections, i.e., the cross sections represented by the solid curve with dots in Fig. 5(b) for H₂ and those represented by the open triangles in Fig. 5(d) for D₂ are not clear at present. The oscillator strengths of each component contributing to the $2s$ -atom formation were obtained by integrating the theoretical curves and difference curves in Fig. 5 in the range of 30–50 eV and the results are summarized in Table I.

Table I shows that the isotope effect that appears in the σ_{2s}^Π cross sections stems mostly from the neutral dissociation of the $Q_2^1 \Pi_u(1, 2)$ states. As mentioned above, substitution to the heavier isotopes results in smaller dissociation yield due to the competition between the neutral dissociation and autoionization. In the course of the discussion on the dissociation dynamics mentioned above, it is expected that the probability of forming the $2s$ atom also changes with the isotopic substitution due to the difference in transition probabilities between two dissociation channels at the avoided crossing mentioned above: the dissociation in D₂ proceeds more adiabatically than in H₂ because the velocity of the relative motion of the two nuclei is smaller for D₂. The latter factor would be a primary cause for the large isotope effect seen in the $Q_2^1 \Pi_u(2)$ component since the theoretical photodissociation cross section via the $Q_2^1 \Pi_u(2)$ state of D₂ does not differ quite so much from the corresponding cross section for H₂ [12,27]. Note that the transitions at the avoided crossings were not taken into account in the theory while the competitions between neutral dissociations and autoionizations were evaluated [12,27]. The present conclusion that the $Q_2^1 \Pi_u(2)$ state of H₂ is likely to result in the $2s$ -atom formation as compared with the same state of D₂ leads to the adiabatic and diabatic correlations as shown in Fig. 7. It is expected that, since dissociations in H₂ proceed

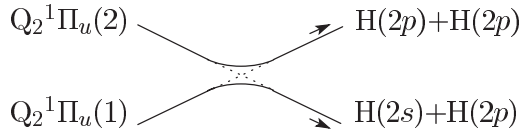


FIG. 7. The adiabatic (solid lines) and diabatic (dotted lines) correlations of the $Q_2 \ ^1\Pi_u(1, 2)$ states derived from the present experimental results (see text).

more diabatically than in D_2 , H_2 [$Q_2 \ ^1\Pi_u(2)$] is more likely to result in $2s + 2p$ than D_2 [$Q_2 \ ^1\Pi_u(2)$] and H_2 [$Q_2 \ ^1\Pi_u(1)$] is more likely to result in $2p + 2p$ than D_2 [$Q_2 \ ^1\Pi_u(1)$]. The correlations shown in Fig. 7 are not consistent with the BL correlations but are consistent with the correlations adopted by Glass-Maujean and coworkers [4,21,30]. It should be noted that the nonadiabatic transition during the dissociation of the $Q_2 \ ^1\Pi_u(1)$ state proposed in the present study would not affect the framework of the angular correlation theory of our group [32] since the transition takes place between the states with the same electronic symmetry.

The ratios of the cross sections, $R(E) \equiv \sigma_{2s}(E)/\sigma_{2p}(E)$, for H_2 and D_2 are shown in Fig. 8 together with those for H_2 in the previous experimental [21] and theoretical [19] studies. The previous ratio $R(E)$ has its maximum around 37 eV while the peak energy in the present one for H_2 is lower by at least 1 eV. The broad peak in the theoretical ratio $R(E)$ in the range 30–36 eV seems to originate from the contribution from the $Q_2 \ ^1\Pi_u(1)$ state of H_2 in the σ_{2s} cross section since the theory includes the $Q_2 \ ^1\Pi_u(1)$ state in the $2s$ -atom formation around this energy with the negligible contribution of the $Q_1 \ ^1\Sigma_u^+(1)$ state [see Figs. 5(a) and 5(b)] while it includes the $Q_1 \ ^1\Sigma_u^+(2)$, $Q_1 \ ^1\Pi_u(1)$, $Q_2 \ ^1\Sigma_u^+(1-6)$, and $Q_2 \ ^1\Pi_u(1-7)$ states for the $2p$ -atom formation around this energy [12,19,27]. The theoretical peak ranging from 30 to 36 eV is seen in the

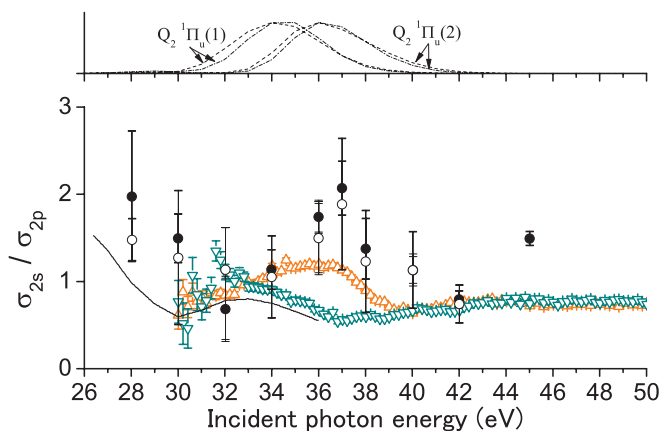


FIG. 8. (Color online) The cross-section ratio $R \equiv \sigma_{2s}/\sigma_{2p}$; (up-triangles) present results for H_2 ; (down-triangles) present results for D_2 ; (open and solid circles) previous experimental results for H_2 [21]; (solid curve) theoretical result for H_2 [19]. The theoretical photodissociation cross sections due to the $Q_2 \ ^1\Pi_u(1)$ and $Q_2 \ ^1\Pi_u(2)$ doubly excited states are also shown in the upper part of the figure with their maxima being normalized; (dashed curves) those for H_2 ; (dot-dashed curves) those for D_2 .

experimental ratio for D_2 , indicating the dominant contribution from the $Q_2 \ ^1\Pi_u(1)$ state in the σ_{2s} cross sections for D_2 . On the other hand, the peak in the present $R(E)$ curve for H_2 is similar in shape to the photodissociation profile due to the $Q_2 \ ^1\Pi_u(2)$ state rather than that due to the $Q_2 \ ^1\Pi_u(1)$ state, which may support the discussion above, suggesting the large contribution of the $Q_2 \ ^1\Pi_u(2)$ state in the σ_{2s}^Π cross section for H_2 . Interestingly, the large isotope effect seen in the present $R(E)$ curves for H_2 and D_2 lies in the range 30–40 eV which is almost identical to the energy range of the photodissociation profiles of the $Q_2 \ ^1\Pi_u(1)$ and $Q_2 \ ^1\Pi_u(2)$ states as shown in the upper part of Fig. 8.

IV. CONCLUSION

We have measured the cross sections for the formation of metastable atomic hydrogen in the $2s$ state in photoexcitation of H_2 and D_2 in the range of the doubly excited states, with the symmetry of the electronic states, $^1\Sigma_u^+$ or $^1\Pi_u$, being selected. For both H_2 and D_2 the cross sections for the $^1\Pi_u$ symmetry, σ_{2s}^Π , were much larger than those for the $^1\Sigma_u^+$ symmetry, σ_{2s}^Σ . The precursor doubly excited states contributing to the formation of the metastable hydrogen were discussed with the help of the best available theory [12,27]. It has been found that the lowest $Q_2 \ ^1\Pi_u$ doubly excited state, the $Q_2 \ ^1\Pi_u(1)$ state, makes a large contribution in the σ_{2s}^Π cross sections for both H_2 and D_2 . However, the theory did not reproduce the cross sections in the range of 32–46 eV, which is probably due to higher doubly excited states in the Q_2 , Q_3 , and Q_4 series. What is missing in the theory would be nonadiabatic transitions between the doubly excited states during dissociations. We found large contributions of the $Q_2 \ ^1\Pi_u(1)$ state to the $2p$ -atom formation and the two $2p$ -atoms formation as well as the $2s$ -atom formation. This finding would be evidence of the nonadiabatic transition between two dissociation pathways into $H(2s) + H(n=2)$ and $H(2p) + H(2p)$. The nonadiabatic transition between the $Q_2 \ ^1\Pi_u(1)$ and $Q_2 \ ^1\Pi_u(2)$ states has been discussed and the adiabatic and diabatic correlations for these doubly excited states are as shown in Fig. 7. It is noted that the σ_{2s}^Σ cross sections in the range 31–46 eV and σ_{2s}^Π cross sections in the range 36–41 eV remain unrevealed.

ACKNOWLEDGMENTS

The authors thank Professor J. L. Sanz-Vicario for the helpful discussion and sending us the unpublished data. The authors also thank Dr. J. R. Machacek for sending us their numerical data. The experiment was carried out under the approval of Photon Factory Program Advisory Committee for Proposal Nos. 2008G107 and 2008G660. This work was partially supported by Grants-in-Aid for Scientific Research (C) (Nos. 19550011 and 22550008) from the Japan Society for the Promotion of Science. T.O. wishes to acknowledge the financial support by the Matsuo Foundation and Reimei Research Promotion Project of the Japan Atomic Energy Agency.

- [1] J. N. Bardsley, *J. Phys. B* **1**, 349 (1968).
- [2] I. Sánchez and F. Martín, *Phys. Rev. A* **57**, 1006 (1998).
- [3] N. Kouchi, M. Ukai, and Y. Hatano, *J. Phys. B* **30**, 2319 (1997).
- [4] M. Glass-Maujean and H. Schmoranzer, *J. Phys. B* **38**, 1093 (2005).
- [5] I. Sánchez and F. Martín, *J. Chem. Phys.* **106**, 7720 (1997).
- [6] I. Sánchez and F. Martín, *J. Chem. Phys.* **110**, 6702 (1999).
- [7] T. E. Sharp, *At. Data* **2**, 119 (1971).
- [8] T. Odagiri, N. Uemura, K. Koyama, M. Ukai, N. Kouchi, and Y. Hatano, *J. Phys. B* **29**, 1829 (1996).
- [9] N. Uemura, T. Odagiri, Y. Hirano, Y. Makino, N. Kouchi, and Y. Hatano, *J. Phys. B* **31**, 5183 (1998).
- [10] F. Martín, *J. Phys. B* **32**, L181 (1999).
- [11] L. Ishikawa, T. Odagiri, K. Yachi, N. Ohno, T. Tsuchida, M. Kitajima, and N. Kouchi, *J. Phys. B* **44**, 065203 (2011).
- [12] J. D. Bozek, J. E. Furst, T. J. Gay, H. Gould, A. L. D. Kilcoyne, J. R. Machacek, F. Martín, K. W. McLaughlin, and J. L. Sanz-Vicario, *J. Phys. B* **39**, 4871 (2006); **41**, 039801 (2008); **42**, 029801 (2009).
- [13] M. Misakian and J. C. Zorn, *Phys. Rev. A* **6**, 2180 (1972).
- [14] A. U. Hazi and K. Wiemers, *J. Chem. Phys.* **66**, 5296 (1977).
- [15] S. L. Guberman, *J. Chem. Phys.* **78**, 1404 (1983).
- [16] S. Arai, T. Yoshimi, M. Morita, K. Hironaka, T. Yoshida, H. Koizumi, K. Shinsaka, Y. Hatano, A. Yagishita, and K. Ito, *Z. Phys. D* **4**, 65 (1986).
- [17] M. Glass-Maujean, *J. Chem. Phys.* **85**, 4830 (1986).
- [18] I. Borges Jr., and C. E. Bielschowsky, *Chem. Phys. Lett.* **342**, 411 (2001).
- [19] J. L. Sanz-Vicario, H. Bachau, and F. Martín, *Phys. Rev. A* **73**, 033410 (2006).
- [20] J. J. Spezeski, O. F. Kalman, and L. C. McIntyre, *Phys. Rev. A* **22**, 1906 (1980).
- [21] M. Glass-Maujean, S. Klumpp, L. Werner, A. Ehresmann, and H. Schmoranzer, *J. Phys. B* **37**, 2677 (2004).
- [22] S. Arai, T. Kamosaki, M. Ukai, K. Shinsaka, Y. Hatano, Y. Ito, H. Koizumi, A. Yagishita, K. Ito, and K. Tanaka, *J. Chem. Phys.* **88**, 3016 (1988).
- [23] T. Odagiri, M. Murata, M. Kato, and N. Kouchi, *J. Phys. B* **37**, 3909 (2004).
- [24] T. Odagiri, Y. Kumagai, T. Tanabe, M. Nakano, I. H. Suzuki, M. Kitajima, and N. Kouchi, *Rev. Sci. Instrum.* **81**, 063108 (2010).
- [25] R. N. Zare, *Angular Momentum: Understanding Spatial Aspects in Chemistry and Physics* (John Wiley & Sons, New York, 1988).
- [26] K. Amemiya and T. Ohta, *J. Synchrotron Radiat.* **11**, 171 (2004).
- [27] J. L. Sanz-Vicario (private communication).
- [28] V. Schmidt, *Electron Spectrometry of Atoms Using Synchrotron Radiation* (Cambridge University Press, Cambridge, UK, 1997).
- [29] E. M. García, J. Á. Ruiz, S. Menmuir, E. Rachlew, P. Erman, A. Kivimäki, M. Glass-Maujean, R. Richter, and M. Coreno, *J. Phys. B* **39**, 205 (2006).
- [30] M. Glass-Maujean, H. Frohlich, and P. Martin, *Phys. Rev. A* **52**, 4622 (1995).
- [31] J. R. Machacek, V. M. Andrianarijaona, J. E. Furst, A. L. D. Kilcoyne, A. L. Landers, E. T. Litaker, K. W. McLaughlin, and T. J. Gay, *J. Phys. B* **44**, 045201 (2011).
- [32] H. Miyagi, A. Ichimura, and N. Kouchi, *J. Phys. B* **40**, 617 (2007).
- [33] T. Tanabe, T. Odagiri, M. Nakano, I. H. Suzuki, and N. Kouchi, *Phys. Rev. Lett.* **103**, 173002 (2009).
- [34] T. Tanabe, T. Odagiri, M. Nakano, Y. Kumagai, I. H. Suzuki, M. Kitajima, and N. Kouchi, *Phys. Rev. A* **82**, 040101(R) (2010); **83**, 066102 (2011).
- [35] K. Jänkälä, P. V. Demekhin, S. Heinäsmäki, I. Haar, R. Hentges, and A. Ehresmann, *J. Phys. B* **43**, 065104 (2010).
- [36] M. Iwai, S. Lee, and H. Nakamura, *Phys. Rev. A* **47**, 2686 (1993).
- [37] H. Nakamura and C. Zhu, *Comments At. Mol. Phys.* **32**, 249 (1996).